Reliable Transient Stability-Constrained Optimal Power Flow Analysis Based on Polynomial Chaos Expansion

Xingrui Li, Chengxi Liu, *Senior Member, IEEE,* Youjin Jiang, Yongjian Luo, and Federico Milano, *Fellow, IEEE*

***Abstract*—This paper proposes a reliable and nonintrusive approach for calculating economical operating states and at the same time, maintaining the transient stability of the system. It focuses on providing a preventive control strategy to address transient rotor angle stability and short-term voltage stability issues resulting from severe disturbances. The objective function, steady-state and multiple types transient stability constraints are equivalently and simultaneously reformulated in polynomial expressions of the control variables such that the original differential-algebraic equations in the transient stability-constrained optimal power flow model are eliminated. This reformulation also allows imposing both rotor angle and voltage magnitude bounds that achieve transient stability and reduce the complexity in the optimization stage. A transient constraint reduction strategy is also proposed to address the large number of constraints introduced by the polynomial chaos expansion when transforming multiple types of transient constraints. This strategy enables the elimination of most transient constraints, thereby further simplifying the overall optimization model. The effectiveness of the proposed method is numerically illustrated and validated through the WECC 3-machine 9-bus system and the IEEE 69-machine 300-bus system.**

***Index Terms*—Transient stability-constrained optimal power flow, transient rotor angle stability, short-term voltage stability, polynomial chaos expansion, constraint reduction strategy.**

NOMENCLATURE

A. Abbreviations

AI	Artificial intelligence.
COI	Center of inertia.
DAEs	Differential-algebraic equations.
MAPE	Mean absolute percentage error.
MC	Monte Carlo.
OOP	Optimal operating point.
OPF	Optimal power flow.
PCE	Polynomial chaos expansion.
PCM	Probabilistic collocation method.
SGM	Stochastic Galerkin method.
SR	Stable region.
TDS	Time-domain simulation.
TS	Trajectory sensitivity.
TSC-OPF	Transient stability-constrained OPF.

X. Li, C. Liu, Y. Jiang, and Y. Luo are with School of Electrical Engineering and Automation, Hubei Engineering and Technology Research Center for AC/DC Intelligent Distribution Network, Wuhan University, Wuhan, 430072, China, and X. Li is also with Shenzhen Power Supply Co. Ltd., Shenzhen, 518001, China, and C. Liu is also with Wuhan University Shenzhen Research Institute, Shenzhen, 518057, China.

F. Milano is with School of Electrical and Electronic Engineering, University College Dublin, Dublin, D04V1W8, Ireland.

This work is supported by the National Natural Science Foundation of China under Project U22B20100 and Shenzhen Science and Technology Program (Grant No. JCYJ20250604122544017).

B. Functions

$C(\cdot)$	Cost function.
$\boldsymbol{F}(\cdot)$	Function of dynamic and control variables.
$\boldsymbol{f}(\cdot)$	Differential functions of power system model.
$\boldsymbol{g}(\cdot)$	Algebraic functions of power system model.
$\boldsymbol{h}_s(\cdot)$	Steady-state inequality constraint functions.
$\boldsymbol{h}_t(\cdot)$	Transient inequality constraint functions.
$\boldsymbol{\Gamma}(\cdot)$	Cumulative distribution function.
$\boldsymbol{\Omega}(\cdot)$	Space of variables.

C. Indices

i, j	Index of generators or buses.
c_i	Index of collocation points.
t_i	Index of time steps.

D. Variables

a_i	i-th polynomial coefficient.
$\boldsymbol{H}_\Phi$	Constant matrix obtained from Φ_i and $\boldsymbol{u}_{c_i}$.
P_{Gi}	Active power injection of the i-th generator.
P_{sg}	Active power injection of the generator connected to the reference bus.
$\boldsymbol{x}$	State variables.
$\boldsymbol{y}$	Algebraic variables.
$\boldsymbol{u}$	Control variables.
u_i	i-th control variable.
$\boldsymbol{u}_{c_i}$	i-th set of collocation points.
V_i	Voltage magnitude of bus i.
V_{si}	Voltage magnitude of bus i in the steady state.
$\boldsymbol{z}$	Compact form of $\boldsymbol{x}$ and $\boldsymbol{y}$.
z_{c_i}	System response of i-th set of collocation points.
$z(t_i)$	Actual value of z in the i-th time step.
$\tilde{z}(t_i)$	Estimated value of z in the i-th time step.
$\bar{\delta}_i$	Rotor angle of generator i.
δ_i^{COI}, δ_i	COI rotor angle of generator i.
Φ_i	i-th term polynomial basis of multi-dimensional variables
$\varphi_{i_j}(u_j)$	i_j-th order polynomial basis of u_j.
$\phi_{i_j}(u_j)$	i_j-th order original polynomials of u_j.

E. Parameters

A_i, B_i, C_i	Fuel cost coefficients of the i-th generator.
d	Maximum order of univariate polynomial basis.
$\boldsymbol{h}_s^{\max}, \boldsymbol{h}_s^{\min}$	Upper and lower bounds of $\boldsymbol{h}_s$, respectively.
M_i	Inertia coefficient of generator i.

N	Total degree of polynomial expansion.
N_t	Total number of steps.
n_x, n_y, n_u	The dimension of x, y, u, respectively.
t_f, t_c, t_{end}	Fault occurrence, clearing time and end of the simulation, respectively.
$\boldsymbol{u}^{\max}, \boldsymbol{u}^{\min}$	Upper and lower bound of $\boldsymbol{u}$, respectively.
$V_s^{\max}, V_s^{\min}$	Upper and lower bound of voltage magnitude in steady state, respectively.
$V^{\min}$	Voltage magnitude limit.
$\delta^{\max}$	Rotor angle limit.

F. Sets

$\mathcal{B}$	Set of buses.
$\mathcal{G}$	Set of generators.
$\mathcal{T}, \mathcal{T}_s, \mathcal{T}_c$	Set of total time steps, time steps before fault occurrence and after fault clearing, respectively.

I. Introduction

A. Motivations

The transient stability-constrained optimal power flow (TSC-OPF) is an effective and appropriate tool to identify the preventive control actions that are needed for economical operation and dynamic security of power systems [1]. However, there remain unresolved issues. For example, most existing approaches face significant challenges in efficiently and accurately addressing multiple types of transient constraints simultaneously, such as rotor angles and voltage magnitudes [2]. This limitation often results in a substantial increase in model complexity and computational burden. Moreover, research on the reduction of transient constraint quantities remains limited, particularly in scenarios where the TSC-OPF model incorporates various types of transient constraints. In such cases, the excessive number of transient constraints introduces several potential issues, such as numerical stability and scalability. This work addresses these issues and proposes a reliable TSC-OPF analysis method and corresponding transient constraint reduction strategy.

B. Literature review

The TSC-OPF for preventive control is formulated as a nonlinear optimization problem that includes differential-algebraic equations (DAEs) for considering the system's dynamic behavior and constructing transient constraints. For this reason, conventional programming methods are not feasible for direct application [3]. The solutions to this challenging problem fall into the following five main categories: (i) numerical discretization methods, (ii) shooting methods, (iii) sequential methods, (iv) perturbation methods, and (v) surrogate model methods.

In the numerical discretization methods, the differential equations in the original TSC-OPF model are discretized into large-scale algebraic equations or inequalities, and the reformulated TSC-OPF model is then solved by classical optimization methods. In [3], the single machine equivalent theory is adopted to reduce the original multi-machine model to a two-machine model and then further reduce the latter to a one-machine infinite-bus equivalent. In [4], the N-1 contingency TSC-OPF problem is addressed using a mixed-integer linear programming model combined with successive linear programming, where the dynamics are discretized in the time domain, and the dynamic equations are integrated using the trapezoidal rule. In [5], the rotor angle stability constraints are transformed into algebraic equations using the trapezoidal integration method and the transformed TSC-OPF model integrates pre-fault, fault, and post-fault stages into a unified framework.

The idea of shooting methods is to replace the representation of the system dynamics with time-domain simulations embedded in the optimization process, such that the transient constraints can be directly evaluated from the simulated trajectories. The single shooting (SS) approach performs the simulation over the entire post-disturbance interval as a single integration process and computes the corresponding sensitivities to guide the optimization [6]. The scheme of SS integrates the system dynamics over the entire simulation horizon in a single run and evaluates sensitivities with respect to control variables based on the resulting trajectories. Although conceptually straightforward and relatively easy to implement, SS may suffer from the convergence problem and numerical instability, particularly when state trajectories exhibit divergence or ill-conditioning under severe contingencies. To alleviate the drawbacks above, the multiple shooting (MS) scheme divides the simulation horizon into subintervals, introduces boundary states as optimization variables, and imposes continuity constraints to assemble a complete trajectory [7]. This strategy enhances numerical robustness and convergence by reducing error accumulation in long-horizon integration but increases the computational burden due to repeated simulations and sensitivity evaluations.

Sequential methods reformulate transient stability requirements as active power re-dispatch constraints, and decompose the problem into two subproblems: a conventional OPF augmented with re-dispatch constraints and a transient stability assessment [8]. By sequentially solving the two subproblems, the generation dispatch is progressively adjusted until a transiently stable operating point is obtained. This strategy avoids discretized dynamic constraints, resulting in a problem dimension and computational cost comparable to standard OPF, and markedly lower than those of discretization methods or shooting methods [9]. In [2], the sequential approach is extended to address not only rotor angle stability but also transient voltage drops for the first time. Two projection stages are designed to ensure both transient rotor angle and voltage stability through non-heuristic active power re-dispatch.

The perturbation method is a local linear approximation that consists of observing the system's dynamic response under small perturbations around the equilibrium operating point. In [10], the significance of power generation with respect to rotor angle deviation is approximated using the trajectory sensitivity (TS) technique and generation is then shifted to the least vulnerable generator. However, the accuracy deteriorates significantly when the operating points deviate from the initial one due to the nonlinearity of the system. The advantages of the perturbation method include the ability to provide fast approximations and its relatively

low computational complexity. However, the first-order TS method lacks the ability to capture the nonlinear dynamics of the system. Although increasing the order of TS can improve accuracy by alleviating the approximation error caused by the nonlinearity [11]–[13], the computational complexity increases significantly, especially in large-scale power systems. Besides, when the operating point deviates from the equilibrium point, the precision and effectiveness of preventive control measures could be compromised.

The surrogate model methods build the nonlinear relationship between the system response and the inputs in either explicit or implicit form which is then utilized to reformulate the optimization problem. Artificial intelligence (AI) algorithms constitute an essential subclass of surrogate model-based approaches for solving the TSC-OPF problem. With the rapid advancements in AI techniques, a variety of learning-based methods have been further introduced, such as decision tree techniques [14], support vector machines [15], and artificial neural networks [16]. These methods leverage data-driven approaches to enhance predictive accuracy and problem-solving capabilities across diverse applications. In [17], a deep sigma point processes-assisted chance-constrained method for transient stability preventive control is proposed, addressing stability risks induced by uncertainties in renewable energy and loads. In [18], an ensemble sparse oblique regression tree method is proposed for the optimization of voltage stability-constrained operation. AI algorithms can efficiently handle complex nonlinear relationships inherent in transient stability constraints and accommodate diverse types of constraints simultaneously. However, AI algorithms operate as black-box models, which lack interpretability and, often, trustworthiness, making it challenging to provide insights into the underlying decision-making process and to ensure compliance with operational standards [19].

To deal with the issues above, the polynomial chaos expansion (PCE), which belongs to another subclass of surrogate model methods and depicts the system response using a set of orthogonal polynomials and corresponding coefficients of the inputs [20], is applied. The PCE has all advantages of AI algorithms with respect to numerical discretization and perturbation methods. In addition, the advantages of PCE with respect to AI algorithms are that PCE is free from the dataset and time-consuming offline training process and is reliable as it retains, even if approximated, the model of the system. In [21], the transient rotor angle stability is considered and transient constraints are reformulated using PCE. However, short-term voltage stability is not included. Besides, the core idea of [21] is to add the transformed transient constraints to the conventional OPF model. The power flow equations are still required in the optimization stage which increases the complexity. Moreover, the number of reformulated transient constraints is tremendous because the transformed constraints of all generators at every moment are added, which may cause an excessive computational burden and potentially lead to convergence issues.

C. Contributions

This paper addresses the limitations above and proposes a reliable PCE-based TSC-OPF analysis approach for preventive control where both transient rotor angle stability and short-term voltage stability problems are simultaneously considered. The two main contributions of the paper are as follows.

- A transient constraint reduction strategy based on the estimation of upper and lower bounds of dynamic response is proposed for the first time, addressing the challenge posed by the large number of algebraic inequality constraints resulting from the PCE reformulation.
- A systematic PCE-based approach to explicitly reformulate the original objective function, complicated DAEs constraints of steady-state and transient rotor angle and voltage magnitudes to simple AEs constraints simultaneously. This not only ensures the accuracy of model and constraint estimation but also significantly reduces the computational complexity of the optimization problem.

D. Paper organization

The remainder of the paper is organized as follows. Section II presents the mathematical formulation of TSC-OPF. Section III provides the details of PCE theory and describes the proposed strategy of applying it to transform the DAEs constraints into AEs constraints. The implementation of the proposed formulation in two study cases is described in Section IV. Section V gives the conclusions and proposes future work.

II. TSC-OPF Model Description

A. Formulation of TSC-OPF

The conventional optimal power flow (OPF) aims to minimize a predefined objective function while complying with a set of static physical and operational constraints. The TSC-OPF is a highly nonlinear optimization problem that integrates transient stability constraints in the form of DAEs into the conventional OPF. The generalized model of TSC-OPF is as follows:

$$\min_{\boldsymbol{x}(t),\boldsymbol{y}(t),\boldsymbol{u}} C(\boldsymbol{x}(t),\boldsymbol{y}(t),\boldsymbol{u})\,,\ \forall t\in[0\,,\,t_f)\,, \tag{1}$$

subject to:

$$\dot{\boldsymbol{x}} = \boldsymbol{f}(\boldsymbol{x}(t),\boldsymbol{y}(t),\boldsymbol{u})\,,\ \forall t\in[0\,,\,t_{end}]\,, \tag{2}$$

$$\boldsymbol{0} = \boldsymbol{g}(\boldsymbol{x}(t),\boldsymbol{y}(t),\boldsymbol{u})\,,\ \forall t\in[0\,,\,t_{end}]\,, \tag{3}$$

$$\boldsymbol{h}_s^{\min} \le \boldsymbol{h}_s(\boldsymbol{x}(t),\boldsymbol{y}(t),\boldsymbol{u}) \le \boldsymbol{h}_s^{\max}\,,\ \forall t\in[0\,,\,t_f)\,, \tag{4}$$

$$\boldsymbol{h}_t(\boldsymbol{x}(t),\boldsymbol{y}(t),\boldsymbol{u}) \le 0\,,\ \forall t\in(t_c\,,\,t_{end}]\,. \tag{5}$$

The objective function $C : \mathbb{R}^{n_x+n_y+n_u}\mapsto\mathbb{R}$ represents the operating cost of power production; $\boldsymbol{f} : \mathbb{R}^{n_x+n_y+n_u}\mapsto\mathbb{R}^{n_x}$ are the differential equations; $\boldsymbol{g} : \mathbb{R}^{n_x+n_y+n_u}\mapsto\mathbb{R}^{n_y}$ are the algebraic equations; $\boldsymbol{h}_s$ are the steady-state inequality constraints and $\boldsymbol{h}_s^{\min}$ and $\boldsymbol{h}_s^{\max}$ are the corresponding lower and upper bounds; $\boldsymbol{h}_t$ are the transient inequality constraints; $\boldsymbol{x}\in\mathbb{R}^{n_x}$ is a vector of state variables; $\boldsymbol{y}\in\mathbb{R}^{n_y}$ is a vector of algebraic variables; $\boldsymbol{u}\in\mathbb{R}^{n_u}$ is a vector of control parameters; t_f, t_c, t_{end} are fault occurrence, clearing time and end of simulation, respectively. Equations (2) and (3) model

the dynamic behavior and steady-state power flow balances of power systems, respectively. Equation (4) represents the technical limits including power production of generators and bus voltage magnitudes. Equation (5) includes the transient stability constraints such as maximum acceptable relative rotor angle deviation and bus voltage magnitude fluctuation. The full details of the above TSC-OPF model are given in [3].

B. Transient Stability Criteria

TSC-OPF aims to optimize the power system's equilibrium operating point, achieving both economy and security. From a preventive security perspective, all security limits in both steady-state and transient stages under one or multi-contingency cases are required to be satisfied by only adjusting the pre-contingency control variables $\boldsymbol{u}$.

The rotor angle stability criterion states that the maximum rotor angle deviation during the whole simulation period must be below the instability limit $\delta^{\max}$. To make the criterion more practically meaningful, the center of inertia (COI) framework of rotor angle is utilized:

$$\begin{aligned} \delta_i^{COI}(t) = \bar{\delta}_i(t) - \frac{\sum_{j\in\mathcal{G}} M_j \delta_j(t)}{\sum_{j\in\mathcal{G}} M_j} \\ \leq \delta^{\max}, \forall i \in \mathcal{G}, \forall t \in (t_c, t_{end}]. \end{aligned} \tag{6}$$

For simplification, δ_i stands for δ_i^{COI} in the rest of the paper unless otherwise specified.

In the transient stage, induction motors may decelerate sharply due to voltage fluctuations and even stall if the electrical torque cannot overcome the mechanical load. Then, a large amount of reactive current is required and this substantially further decreases the voltage magnitudes and hinders voltage recovery. Thus, the transient evolution of voltage magnitudes also plays a vital role in transient stability. The short-term voltage stability criterion states that the voltage magnitudes of all buses are greater than a predetermined limit after the fault is cleared:

$$V_i(t) \geq V^{\min}, \forall i \in \mathcal{B}, \forall t \in (t_c, t_{end}]. \tag{7}$$

Traditionally, not only because of the highly nonconvex and nonlinear features but also the additional DAEs constraints (2) and (3) compared to the traditional OPF, it is difficult to solve the TSC-OPF problem, especially when the transient stability criteria include different variables. To address this, the next section introduces the PCE technique to construct a surrogate model that represents the original objective function (1), the steady-state constraints (4) and transient constraints (5) through a set of polynomial equations, thereby reformulating the problem in a tractable polynomial form that implicitly incorporates the DAEs in (2) and (3). Through this reformulation, the overall complexity of the TSC-OPF model is effectively reduced.

III. Reformulation of Transient Stability Constraints Using Polynomial Chaos Expansion

A. Surrogate Model based on Polynomial Chaos Expansion

The overall procedure of the proposed PCE-based TSC-OPF analysis for preventive control of rotor angle stability and short-term voltage stability is summarized in Fig. 1. The proposed framework consists of several sequential parts. Orthogonal polynomial bases are first constructed to provide the functional representation of system responses. Collocation points are then selected and time-domain simulations are performed, from which the PCE surrogate model is established. A transient constraint reduction procedure is subsequently employed to retain only the critical stability constraints. Finally, the reformulated TSC-OPF model is solved by utilizing a nonlinear programming solver.

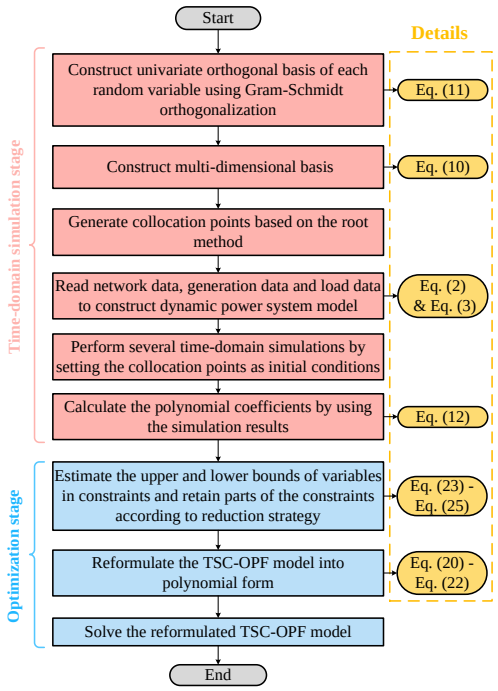

Fig. 1. Flowchart of the proposed PCE-based TSC-OPF method.

As shown in (2) and (3), the system's dynamic behavior of $\boldsymbol{x}(t)$ and $\boldsymbol{y}(t)$ is implicitly related to the control parameters $\boldsymbol{u}$. To derive an explicit relationship, the PCE technique is utilized to build a surrogate model that $\boldsymbol{x}(t)$ and $\boldsymbol{y}(t)$ are expressed using a set of polynomial equations of $\boldsymbol{u}$. To simplify expressions, $\boldsymbol{z}(t) \in \mathbb{R}^{n_x+n_y}$ is used as the compact form of $\boldsymbol{x}(t)$ and $\boldsymbol{y}(t)$ in the remainder of the paper.

Control parameters $\boldsymbol{u}$, representing the generator's active injection, can be adjusted arbitrarily within a predetermined and continuous range. The elements of vector $\boldsymbol{u}$ inherently satisfy two key properties: (i) unbiasedness, meaning that the values of the elements of $\boldsymbol{u}$ are equally likely in their specified ranges; and (ii) independence, indicating that the variations of $\boldsymbol{u}$ are unaffected by external factors or the states of other generators. These properties enable the transition from an interval-based representation to a probabilistic modeling framework. In practice, the elements of $\boldsymbol{u}$ can be regarded as multi-dimensional random variables following uniform distributions with cumulative distribution function $\boldsymbol{\Gamma}(\boldsymbol{u})$ and space $\boldsymbol{\Omega}(\boldsymbol{u})$. The dimension of $\boldsymbol{u}$ refers to the number of controllable generators.

Let $\boldsymbol{z}(t)$ be an implicit function $\boldsymbol{F}(t,\boldsymbol{u})$ of $\boldsymbol{u}$:

$$\boldsymbol{z}(t)=\boldsymbol{F}(t,\boldsymbol{u})\,,\ \forall t\in\mathcal{T}. \tag{8}$$

Note that t changes from a continuous variable to a discrete variable at each simulation step, making the transient constraints in the subsequent optimization process finite.

For a single variable $z(t)$ in $\boldsymbol{z}(t)$, the PCE method is used to construct an explicit relationship between $z(t)$ and $\boldsymbol{u}$ through a series of orthogonal polynomials and corresponding coefficients as follows:

$$z(t)\approx\sum_{i=0}^{N}a_i(t)\Phi_i(\boldsymbol{u})\,,\ \forall t\in\mathcal{T}\,, \tag{9}$$

where $N=\frac{(n_u+d)!}{n_u!d!}-1$.

The set of multi-dimensional basis $\{\Phi_i\}$ is constructed based on univariate basis $\varphi_{i_j}(u_j)$ as:

$$\{\Phi_i\}=\{\varphi_{i_1}(u_1)\varphi_{i_2}(u_2)\cdots\varphi_{i_{n_u}}(u_{n_u})\,,\sum_{j=1}^{n_u}i_j\le d\}\,. \tag{10}$$

To derive the univariate basis $\varphi_{i_j}(u_j)$, Gram-Schmidt orthogonalization [22] is utilized. For u_j, the Gram-Schmidt orthogonalization process constructs a set of orthogonal polynomials $\{\varphi_{0_j}(u_j),\varphi_{1_j}(u_j),\cdots,\varphi_{d_j}(u_j)\}$ from a given independent polynomial set $\{\phi_{0_j}(u_j),\phi_{1_j}(u_j),\cdots,\phi_{d_j}(u_j)\}$. First, the 0-th order polynomials $\varphi_{0_j}(u_j)$ and $\phi_{0_j}(u_j)$ are set to 1. Next, the orthogonal polynomials are obtained iteratively using the following recurrence procedure:

$$\varphi_{j_k}(u_j)=\phi_{j_k}(u_j)-\sum_{i=0}^{k-1}\frac{\langle\phi_{j_k}(u_j),\varphi_{j_i}(u_j)\rangle}{\langle\varphi_{j_i}(u_j),\varphi_{j_i}(u_j)\rangle}\varphi_{j_i}(u_j)\ ,k\ge1\,, \tag{11}$$

where $\langle\cdot,\cdot\rangle$ is the inner product. After the above procedure is implemented to all control variables, the multi-dimensional basis $\{\Phi_i\}$ can be obtained using (10).

B. Probabilistic Collocation method

Once the bases are determined, either the probabilistic collocation method (PCM) [20] or the stochastic Galerkin method (SGM) [23] can then be utilized to calculate the polynomial coefficients a_i in (9). SGM is intrusive, requiring substantial reformulation of the system equations and the solution of high-dimensional deterministic DAEs, which may become intractable for large-scale systems. By contrast, PCM is non-intrusive, as it relies only on the input–output relation of the simulation model and constructs the surrogate through multiple independent runs at collocation points. This feature enables straightforward integration with commercial simulation platforms and allows for efficient parallelization. For these reasons, PCM is adopted in this work.

The collocation point sets $\{\boldsymbol{u}_{c_i}\}$ can be regarded as a set of samples representing the probabilistic features of $\boldsymbol{u}$. The accuracy of approximation results is significantly related to the selected collocation points. Based on the root method [23], the collocation points are selected by the combinations of roots of one higher-order univariate polynomial basis. For example, consider a 2nd-order PCE with random input variable u following uniform distributions. The collocation points are selected based on the roots of the corresponding one-order-higher orthogonal polynomial of univariate random variable, namely the 3rd-order Legendre polynomial. The 3rd-order Legendre polynomial is given by $\varphi_3(u)=5u^3-3u$ and the roots are $\{-\sqrt{3/5},0,\sqrt{3/5}\}$. For multi-dimensional random inputs, such as when there are n_u random inputs, the total number of collocation point combinations formed by the roots is 3^{n_u}.The number of collocation sets equals the number of polynomial bases $(N+1)$, which is also the number of required time-domain simulations to calculate the corresponding system dynamic response z_{c_i}. To determine the $(N+1)$ polynomial coefficients in the PCE model, $(N+1)$ subsets are selected randomly from the complete sets. Then, the polynomial coefficients $a_i(t)$ are calculated based on the collocation point sets $\boldsymbol{u}_{c_i}$ and the system response z_{c_i} by solving the following linear equation:

$$\begin{aligned}&\left[a_0(t),a_1(t),\cdots,a_N(t)\right]^{\mathrm{T}}\\&=\boldsymbol{H}_{\Phi}^{-1}\left[z_{c_1}(t),z_{c_2}(t),\cdots,z_{c_{N+1}}(t)\right]^{\mathrm{T}}\,,\quad\forall t\in\mathcal{T}\,,\end{aligned} \tag{12}$$

where $\boldsymbol{H}_{\Phi}$ is a constant matrix obtained from the basis Φ_i and collocation point sets $\boldsymbol{u}_{c_i}$:

$$\boldsymbol{H}_{\Phi}=\begin{bmatrix}\Phi_0(\boldsymbol{u}_{c_1})&\Phi_1(\boldsymbol{u}_{c_1})&\cdots&\Phi_N(\boldsymbol{u}_{c_1})\\\Phi_0(\boldsymbol{u}_{c_2})&\Phi_1(\boldsymbol{u}_{c_2})&\cdots&\Phi_N(\boldsymbol{u}_{c_2})\\\vdots&\vdots&\vdots&\vdots\\\Phi_0(\boldsymbol{u}_{c_{N+1}})&\Phi_1(\boldsymbol{u}_{c_{N+1}})&\cdots&\Phi_N(\boldsymbol{u}_{c_{N+1}})\end{bmatrix}.$$

C. Transformation of the Objective Function and Constraints

First, we define the objective function in this paper as the operating cost of power production:

$$C(P_{Gi})=\sum_{i\in\mathcal{G}}(A_iP_{Gi}^2+B_iP_{Gi}+C_i)\,. \tag{13}$$

Regarding the selection of control variables, in the proposed approach, the power flow equations are resolved in advance during the simulation stage. Specifically, the output of the generator at the reference bus P_{sg} is treated as a system response determined by the outputs of the other generators instead of a control variable, and its PCE representation is derived accordingly. This allows the objective function to be expressed explicitly in terms of control variables and PCE coefficients, without the need to include power flow constraints in the subsequent optimization problem. Meanwhile, the optimality of the solution is not affected. To transform the P_{sg} in the objective function, (9) is utilized as:

$$P_{sg}(t)\approx\sum_{j=0}^{N}a_j^{(P_{sg})}(t)\Phi_j(\boldsymbol{u})\,,\ \forall t\in\mathcal{T}_s\,. \tag{14}$$

So, the transformed objective function is of the polynomial coefficients $a_j^{(P_{sg})}$ and control variables $\boldsymbol{u}$. Note that since P_{sg} is determined by the outputs of the controllable generators, P_{sg} does not satisfy the independence assumption required for the probabilistic modeling of input variables.

Next, we reformulate the steady-state constraints using (9). For example, the voltage magnitudes in the steady-state stage can be expressed as:

$$V_{si}(t) \approx \sum_{j=0}^{N} a_j^{(V_{si})}(t)\Phi_j(\boldsymbol{u})\,, \forall i \in \mathcal{B}\,,\, \forall t \in \mathcal{T}_s\,. \tag{15}$$

Accordingly, the steady-state voltage magnitude constraints are:

$$V_s^{\min} \leq \sum_{j=0}^{N} a_j^{(V_{si})}(t)\Phi_j(\boldsymbol{u}) \leq V_s^{\max}\,, \forall i \in \mathcal{B}\,,\, \forall t \in \mathcal{T}_s\,. \tag{16}$$

By reformulating the objective function and steady-state constraints, the power flow equations in the steady-state stage are replaced and eliminated. Since the original power flow equations are implicit functions of $\boldsymbol{u}$, while the reformulated objective function and steady-state constraints are explicit, the complicity of the optimization model is reduced.

We further express the system dynamic responses $\boldsymbol{z}(t)$ to polynomial form. The transient inequality constraints (6) and (7) can be transformed into polynomials correspondingly:

$$\delta_i(t) \approx \sum_{j=0}^{N} a_j^{(\delta_i)}(t)\Phi_j(\boldsymbol{u}) \leq \delta^{\max}\,,\, \forall i \in \mathcal{G}\,,\, \forall t \in \mathcal{T}_c\,, \tag{17}$$

$$V_i(t) \approx \sum_{j=0}^{N} a_j^{(V_i)}(t)\Phi_j(\boldsymbol{u}) \geq V^{\min}\,,\, \forall i \in \mathcal{B}\,,\, \forall t \in \mathcal{T}_c\,. \tag{18}$$

In this way, the DAEs of the TSCOPF model are completely eliminated since (17) and (18) contain all dynamic information of the rotor angle and voltage magnitude in the transient process, respectively. Therefore, the TSC-OPF model can be reformulated in compact form as:

$$\min_{\boldsymbol{u}} C(\boldsymbol{a}^{(P_{sg})}(t), \boldsymbol{u})\,,\, \forall t \in \mathcal{T}_s\,, \tag{19}$$

subject to:

$$\boldsymbol{h}_s^{\min} \leq \boldsymbol{h}_s(\boldsymbol{a}^{(z)}(t), \boldsymbol{u}) \leq \boldsymbol{h}_s^{\max}\,,\, \forall t \in \mathcal{T}_s\,, \tag{20}$$

$$\boldsymbol{h}_t(\boldsymbol{a}^{(z)}(t), \boldsymbol{u}) \leq 0\,,\, \forall t \in \mathcal{T}_c\,. \tag{21}$$

An advantage of the proposed method is that the objective function and all constraints are expressed in an explicit polynomial form. As a result, the system parameters, power flow equations, and system dynamic equations are no longer required to be input and modeled in the optimization solver which significantly reduces the complexity of the model. The DAEs constraints (2) and (3), which are not directly solvable in commercial optimization software, are eliminated and implicitly embedded within the transformed model. This reformulation results in a set of explicit polynomial inequality constraints (20) and (21), which can be effectively solved using commercial optimization software equipped with nonlinear solvers.

Regarding the quadratic property of the transformed objective function (19), when the 1st-order PCE is applied, the mapping from the polynomial coefficients to the generator outputs is linear, and the transformed objective function (20) remains quadratic. For the 2nd-order or higher expansions, the polynomial basis introduces higher-order terms, which result in the transformed objective no longer being quadratic. As for convexity, although the cost function remains quadratic for the 1st-order expansion, the overall TSC-OPF model is inherently non-convex due to the power flow equations and transient stability constraints. This non-convexity persists in the surrogate model (19)-(21) for higher-order expansions. In practice, high-quality solutions can be obtained by applying local nonlinear solvers with multiple initial guesses, including physically meaningful ones such as the current operating point or typical system setups.

In this paper, the CONOPT solver in GAMS is utilized to solve the reformulated optimization problem. Moreover, the construction process of the surrogate model is non-intrusive and commercial simulation software can be directly utilized to build the surrogate model. Only predetermined collocation points and system dynamic response are needed to derive the polynomial expressions (9) which means the modification of the built-in models or numerical solvers is not required. The advantages above ensure ease of use for power utilities. Note that since PCE is applied to model the dynamic response at each time instant, it provides a versatile framework to address additional objectives. For instance, by imposing bounds on the difference between the system's response at two arbitrary time points and ensuring that the variation remains within a predefined threshold, the transient fluctuations can be mitigated.

D. Reduction Strategy of Transient Stability Constraints

Converting the transient stability constraints into inequality constraints leads to a high number of inequalities. The computational burden of solving this high-dimensional polynomial optimization problem can become untractable. To solve this issue, we propose a strategy to reduce the number of constraints, based on the estimation of the upper and lower bounds of $\delta_i(t)$ and $V_i(t)$. In [20] and [24], the expectation and standard deviation of the system response are obtained from the PCE model, and the corresponding bounds are subsequently determined using the 3σ criterion, which assumes that nearly all samples lie within three standard deviations from the mean. Nonetheless, notable discrepancies arise between the estimated and actual upper and lower bounds, particularly near the inflection points of the response curves. This discrepancy primarily results from the fact that the 3σ rule presumes a Gaussian distribution of the samples, whereas the actual distribution of system response deviates from any standard form due to the inherent nonlinearities of the system. In addition, inaccuracies in the approximated expectation and standard deviation employed within the 3σ rule further contribute to the observed estimation errors.

Instead of using the expectation and standard deviation that has been utilized in other works (see, e.g., [20], [24]), we derive the upper and lower bounds of $\delta_i(t)$ and $V_i(t)$ at each time step directly by solving optimization problems where the objective functions are minimizing or maximizing the polynomial expressions of transient rotor angles (17) and voltage magnitudes (18) and the constraints are the closed intervals $[\boldsymbol{u}^{\min}, \boldsymbol{u}^{\max}]$. Then, only binding constraints are included in the transformed TSC-OPF model (19) to (21).

The bounds of transient rotor angles and voltages are determined by solving the following optimization problems, respectively:

$$\min_{\boldsymbol{u}} \text{ or } \max_{\boldsymbol{u}} \sum_{j=0}^{N} a_j^{(\delta_i)}(t)\Phi_j(\boldsymbol{u})\,,\ \forall i \in \mathcal{G}\,,\ \forall t \in \mathcal{T}_c\,, \tag{22}$$

or:

$$\min_{\boldsymbol{u}} \text{ or } \max_{\boldsymbol{u}} \sum_{j=0}^{N} a_j^{(V_i)}(t)\Phi_j(\boldsymbol{u})\,,\ \forall i \in \mathcal{B}\,,\ \forall t \in \mathcal{T}_c\,, \tag{23}$$

subject to:

$$\boldsymbol{u}^{\min} \le \boldsymbol{u} \le \boldsymbol{u}^{\max}\,. \tag{24}$$

Note that the proposed reduction strategy is most effective if a small subset of rotor angles or voltage magnitudes exceed their limits during specific time intervals. This is however the most common situation and it is what we have observed to happen in all scenarios that we have considered while preparing this work. In addition, the applicability of this approach relies on the accuracy of the underlying surrogate model, which guarantees that the eliminated constraints correspond to states with zero probability of violation. Therefore, while the strategy effectively reduces complexity, its validity is inherently linked to the surrogate model's representation accuracy. Moreover, given that each optimization model operates independently, a parallel computing framework can be leveraged to accelerate the computational process.

Finally, note that the stability of the optimization results is determined by the accuracy of the PCE-based surrogate model, rather than the proposed reduction strategy of transient stability constraints. The constraints eliminated by the proposed reduction strategy are redundant, meaning that, within the admissible range of control variables, the PCE-represented voltage and rotor angle trajectories never violate their limits. Consequently, removing these constraints neither alters the stable region nor changes optimization results.

E. Diagram for Illustration

The diagram of the proposed transient constraint reduction strategy and the stable region estimation are shown in Fig. 2. In this simple example, two control variables, u_1 and u_2, are considered, with the constraints consisting of steady-state constraints h_{s1} and h_{s2}, as well as transient constraints corresponding to h_{t1} at times t_m and t_n, and h_{t2} at times t_i and t_j. First, taking the transient constraint h_{t1} as an example, its upper and lower bounds can be estimated by solving the optimization model defined by (22) to (24). As shown in Fig. 2, at time t_m, the lower bound of h_{t1} is below its limit $h_{t1}^{\min}$, indicating that inappropriate values of the control variables u_1 and u_2 may result in a violation of the transient constraint. Thus, the constraint on h_{t1} at t_m is identified as a critical constraint. In contrast, the constraint on h_{t1} at t_n is considered a redundant constraint.

To intuitively illustrate the distinction between critical and redundant constraints, the probability density of h_{t1} at t_m and t_n is also depicted in Fig. 2. The probability density of h_{t1} is derived by applying the Monte Carlo method to its polynomial

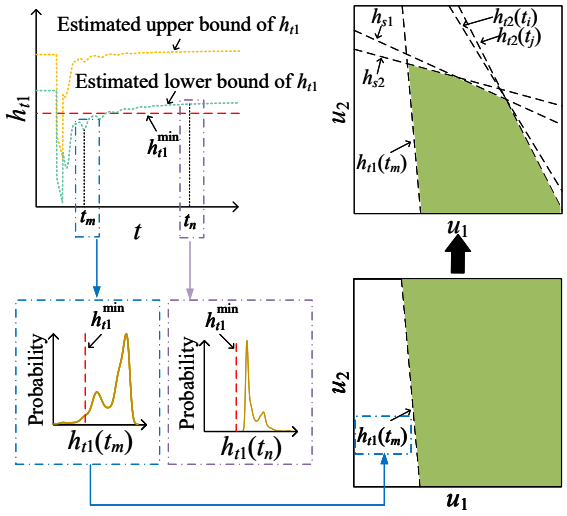

Fig. 2. Transient constraint reduction and stable region estimation process.

expression [25]. The probability distribution shows that h_{t1} is at risk of violating its limit at t_m, whereas no such risk exists at t_n. Based on the proposed constraint reduction strategy, only critical constraints, such as the constraint $h_{t1}(t_m)$, are retained, while redundant constraints, such as $h_{t1}(t_n)$, are discarded. Within the domain of the control variables, the inequality $h_{t1}(t_m) \ge h_{t1}^{\min}$ defines a stability region that satisfies the constraint on h_{t1} at t_m.

The same process is applied to transient constraint h_{t2}, allowing critical constraints, such as $h_{t2}(t_i)$ and $h_{t2}(t_j)$, to be identified. The impact of steady-state constraints h_{s1} and h_{s2} can be determined by solving the inequalities $h_{s1}^{\min} \le h_{s1} \le h_{s1}^{\max}$ and $h_{s2}^{\min} \le h_{s2} \le h_{s2}^{\max}$. Finally, the stable region is depicted by taking the intersection of steady-state constraints with the retained critical transient constraints.

Note that we consider one single harmful contingency in the rest of the manuscript. However, multi-contingency scenarios can be readily considered by adding (21) to the transformed TSC-OPF model for each contingency. In what follows, only single-contingency cases are illustrated.

IV. Case Studies

In this section, we apply the proposed PCE-based TSC-OPF method in the WECC 3-machine, 9-bus system [26] and the IEEE 69-machine, 300-bus system [27]. In both case studies, the detailed 6-order generator model, excitation, and turbine system [28] are considered. The 9-bus system is presented to illustrate the features of the PCE method by comparing the accuracy, reliability, and cost with the 2nd-order TS [13], while the 300-bus system serves to illustrate the robustness of the proposed method when applied to a larger system with more constraints and more state and algebraic variables that potentially violate the constraints.

All simulations are carried out using Matlab R2023a and GAMS 23.8.1 on a laptop with Intel Ultra 5 125H (4.5GHz) and 32 GB RAM. The power flow results for the initialization of time-domain simulations are calculated by MATPOWER 7.1 [29]. The time-domain simulations are carried out based

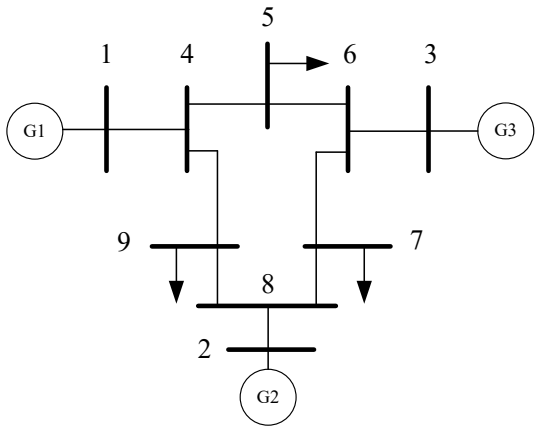

Fig. 3. Topology of the 9-bus system.

on modified PSDAT [28], and the time step of numerical integration is 0.01 s. The TSC-OPF problem is finally solved using CONOPT in GAMS.

A. WECC 9-Bus System

This case serves to compare the accuracy, stability, and cost. The full static and dynamic data of the WECC 3-machine, 9-bus system can be found in [29] and [28], respectively. The whole time-domain simulation time is 5 s, whereas a three-phrase fault occurs at 0.5 s on bus 9 and is cleared after 0.15 s by tripping line 9-4. The single-line diagram of the 9-bus system is shown in Fig. 3.

The steady-state constraints are set as the voltage magnitudes of PQ buses are within the limits of $[0.95, 1.05]$ p.u. The transient rotor angle and voltage constraints are $\delta^{\max} = 100^\circ$ [30] and $V^{\min} = 0.8$ p.u. [31], respectively. Note that in this case, due to the system parameters and fault settings, by only adjusting P_{G2} and P_{G3}, the voltage magnitudes are inevitably below $V^{\min}$ for a period of time after the fault is cleared. Thus, following the work of [1], the acceptable maximum duration of the voltage violation t_d is introduced in this case and t_d is set to 0.75 s. This setting is based on the control capability of the implemented control measures, ensuring that the chosen duration aligns with the system's ability to effectively mitigate disturbances. It is worth noting that t_d is not a fixed parameter; rather, it can be adapted according to different system conditions and operational requirements, thereby providing flexibility in accommodating diverse grid codes or reliability standards. The cost coefficients are $[A_1, A_2, A_3]^{\mathrm{T}} = [0.0525, 0.0175, 0.0275]^{\mathrm{T}}$, $[B_1, B_2, B_3]^{\mathrm{T}} = [0.3, 0.25, 0.25]^{\mathrm{T}}$, $[C_1, C_2, C_3]^{\mathrm{T}} = [37.5, 75, 33.75]^{\mathrm{T}}$, which are modified from the benchmark in [29] to introduce a more distinct difference in the optimal operating points obtained by different methods.

To quantitatively evaluate and compare the accuracy, the mean absolute percentage error (MAPE) e_z is used:

$$e_z = \sum_{i=1}^{N_t} \left| \frac{z(t_i) - \tilde{z}(t_i)}{z(t_i)} \right| \frac{100}{N_t}\% . \tag{25}$$

Note that the reason for choosing MAPE as the index is that it normalizes errors by the magnitude of actual values, providing a percentage-based measure that is scale-independent and intuitive. Additionally, the use of MAPE aligns with established practices in the literature, such as [21], where it has been employed effectively to compare the accuracy.

For the discussion presented in this subsection, we consider the active power injection $P_{G2} \in [100, 170]$ MW of generator 2 and $P_{G3} \in [50, 120]$ MW of generator 3 as the control variables, while bus 1 is the reference bus. The rotor angle of generator 2 (δ_2) and the voltage magnitude of bus 9 (V_9) are selected as representatives since they may violate the stability constraints during the simulation. The initial equilibrium operating point (OP) is $\boldsymbol{P}_{G0} = [P_{G20}, P_{G30}]^{\mathrm{T}} = [135, 85]^{\mathrm{T}}$ MW for the 2nd-order TS. Then, the OPs are set from $80\%\boldsymbol{P}_{G0}$ to $120\%\boldsymbol{P}_{G0}$ to test the estimated accuracy for both PCE and the 2nd-order TS. The actual trajectories are obtained using the original DAEs which are set as benchmarks.

The MAPE comparison of δ_2 and V_9 is summarized in Tables I and II, respectively. For the 2nd-order TS, the estimation error increases as the OPs get farther away from $\boldsymbol{P}_{G0}$, as expected. The reason is that though the 2nd-order TS takes the nonlinearity of the system response into consideration, the approximation model is still constructed based on small perturbations around the initial equilibrium point, that is, $\boldsymbol{P}_{G0}$. Consequently, the farther the OPs are from $\boldsymbol{P}_{G0}$, the worse the accuracy caused by the system nonlinearity. In contrast, the accuracy of PCE remains stable when the OP changes. Because the probabilistic density function is considered rather than one single OP. Also, in the 3rd-order PCE, the inherent nonlinear characteristics of the system are more accurately preserved than in the 2nd-order TS which leads to higher accuracy. With the order of PCE increases from 1 to 3, the accuracy improves significantly. The observed improvement in accuracy with increasing expansion order reflects the inherent convergence property of the PCE. Specifically, as the expansion order is raised, the PCE approximation increasingly captures the underlying functional mapping between the input uncertainties and system responses with higher accuracy. Tables I and II reflect the superiority of the proposed method in terms of accuracy for trajectory estimating, especially when OPs are far from $\boldsymbol{P}_{G0}$.

TABLE I
MAPE OF TRAJECTORIES OF δ_2 IN THE 2ND-ORDER TS AND DIFFERENT ORDERS OF PCE

Method	e_{δ_2}			
	$80\%\boldsymbol{P}_{G0}$	$90\%\boldsymbol{P}_{G0}$	$110\%\boldsymbol{P}_{G0}$	$120\%\boldsymbol{P}_{G0}$
2nd-order TS	1.03%	0.97%	1.01%	1.05%
PCE, d=1	1.15%	1.63%	1.52%	1.48%
PCE, d=2	0.83%	1.01%	0.71%	1.03%
PCE, d=3	0.45%	0.14%	0.30%	0.23%

The evolution of error of δ_2 and V_9 using the 2nd-order TS and PCE when OP is $80\%\boldsymbol{P}_{G0}$ are shown in Fig. 4. Note that the vertical axis represents the general error rather than specifically the MAPE. The error of PCE decreases as the order increases, as expected. Meanwhile, the accuracy of trajectory estimation affects the determination of stability boundaries, thus affecting the performance of the optimization results.

TABLE II
MAPE OF TRAJECTORIES OF V_9 IN THE 2ND-ORDER TS AND DIFFERENT ORDERS OF PCE

Method	e_{V_9}			
	$80\%\boldsymbol{P}_{G0}$	$90\%\boldsymbol{P}_{G0}$	$110\%\boldsymbol{P}_{G0}$	$120\%\boldsymbol{P}_{G0}$
2nd-order TS	0.12%	0.10%	0.09%	0.26%
PCE, d=1	0.11%	0.15%	0.19%	0.37%
PCE, d=2	0.09%	0.13%	0.12%	0.30%
PCE, d=3	0.04%	0.01%	0.02%	0.02%

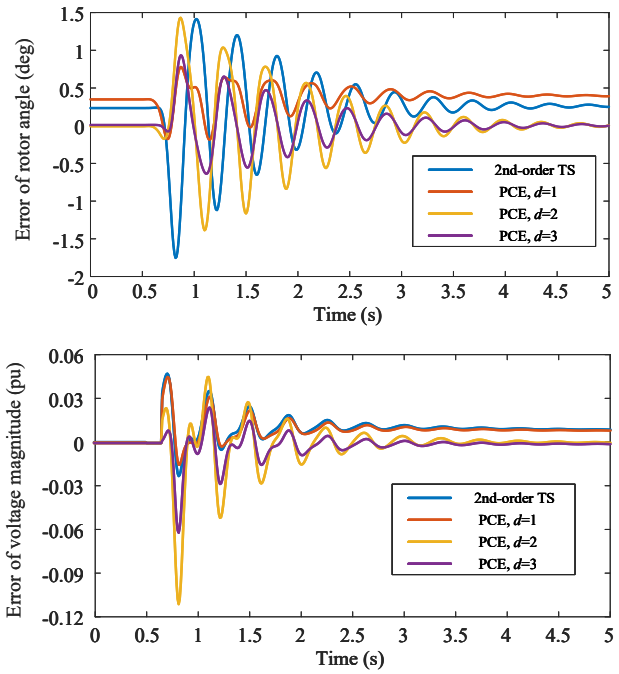

Fig. 4. Error comparison of the 2nd-order TS and PCE when OP is $80\%\boldsymbol{P}_{G0}$. Upper panel: δ_2; Lower panel: V_9.

The trajectories of the Monte Carlo (MC) method and the estimated upper and lower bounds obtained from the 2nd-order TS and PCE are shown in Fig. 5. The input data sets of MC are randomly generated within the ranges of P_{G2} and P_{G3}. The expansion order of PCE is set to 3. For PCE, the 3σ rule and the proposed strategy based on optimization methods are utilized to estimate the bounds. It is observed that the bounds of 2nd-order TS are more accurate than the bounds obtained by the 3σ rule, while the proposed strategy is of the highest accuracy among these three methods. In addition, when the constraint reduction strategy is adopted, if the estimated interval is larger than the actual one, such as the bounds of PCE using the 3σ rule, then the final optimization step contains redundant and ineffective constraints which may lead to excessive computational burden. Conversely, if the estimated interval is too small, then there may be too few constraints in the optimization process, resulting in the final optimized OP violating the stability constraint.

Table III shows the number of transient constraints before and after applying the proposed constraint reduction strategy. It is clear that the proposed strategy reduces the number of transient constraints significantly. The difference in different orders of PCE is on account of the accuracy of the constructed surrogate model. The higher the accuracy of the surrogate

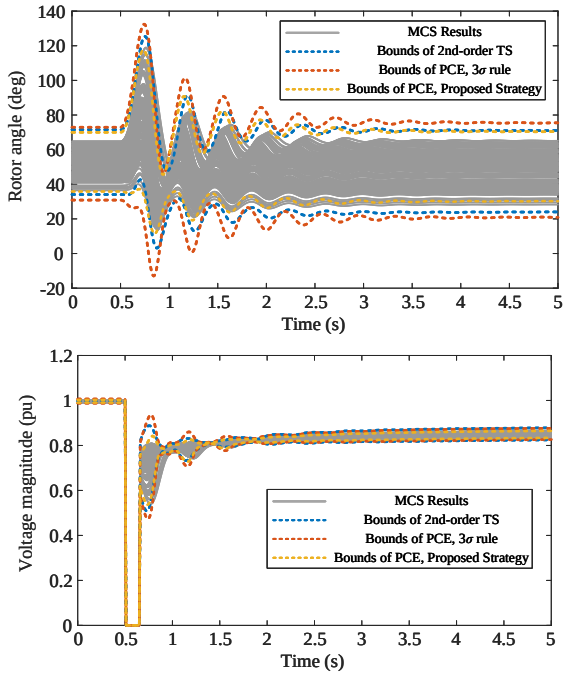

Fig. 5. MC trajectories and estimated bounds of the 2nd-order TS and PCE. Upper panel: δ_2; Lower panel: V_9.

model, the more effective the proposed strategy.

TABLE III
COMPARISON BEFORE AND AFTER APPLYING TRANSIENT CONSTRAINT REDUCTION STRATEGY

Method	Number of transient constraints			
	δ		V	
	Before	After	Before	After
PCE, d=1		40		19
PCE, d=2	1305	33	3375	12
PCE, d=3		27		15

Since the constraints of TSC-OPF are transformed into the explicit polynomial form using the proposed method as in (20) and (21), the stable region (SR) of PCE can be estimated as shown in Fig. 6. For MC and the collocation points of PCE, an OP is unstable if at least one stability constraint is violated, either in the steady state or transient process, and either in terms of rotor angle or voltage magnitude, otherwise, it is stable. The accuracy of the estimated SR increases as the expansion order of PCE increases, as expected. Moreover, it can be observed that the collocation points include both stable and unstable operating conditions. The essential requirement is that these points collectively provide sufficient coverage of the input space, thereby enabling the PCE to accurately capture the functional relationship between the control variables and the system responses. Note also that, if unstable OPs are included in the SR, the final results of optimization might lead to instability. In contrast, if stable OPs are mistakenly classified outside SR, the results could be too conservative and uneconomical.

To further compare the optimization performance, the decision tree (DT) method is also considered [32]. Table IV provides the optimal operating point (OOP) and corresponding

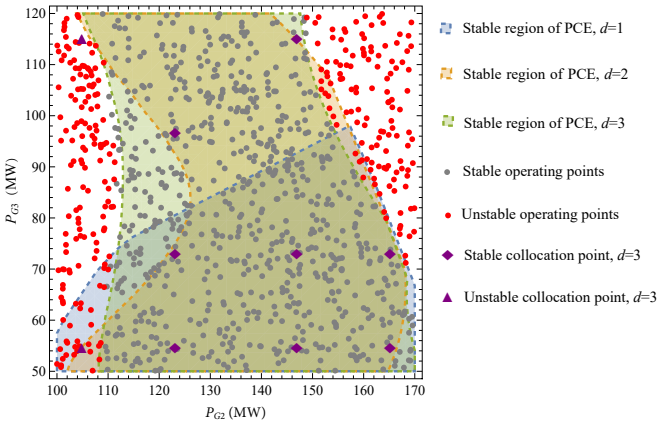

Fig. 6. Stable regions estimated by PCE and stability of MC operating points.

cost obtained from the base OPF, DT, the 2nd-order TS, and different orders of PCE. Also, whether the rotor angle or voltage curves under the given OOP are stable is presented. The base OPF case contains only the steady-state constraints. Though it is the most economical one, the transient stability is not satisfied under this OOP. The OOP of PCE when $d = 2$ achieves rotor angle stability while failing to maintain voltage stability. This means in this case, a higher order of PCE is needed to capture the boundaries of voltage than rotor angles. The main reason is that voltage undergoes a step change after the occurrence and clearing of the fault, leading to stronger nonlinearity. Although both 3rd-order PCE and DT satisfy the transient stability constraints on rotor angle and voltage magnitude, 3rd-order PCE attains a lower generation cost, indicating a more accurate estimation of the stability boundary.

TABLE IV
COMPARISON OF OPTIMIZATION RESULTS

Method	P_{G1} (MW)	P_{G2} (MW)	P_{G3} (MW)	Cost ($/h)	Stability δ	Stability V
Base OPF	56.26	161.05	103.00	1140.93	✗	✗
DT	62.09	149.39	108.51	1146.06	✓	✓
2nd-order TS	62.04	151.19	106.76	1144.87	✓	✗
PCE, $d = 1$	64.54	157.31	98.05	1145.56	✗	✗
PCE, $d = 2$	62.08	153.17	104.74	1143.96	✓	✗
PCE, $d = 3$	61.89	149.96	108.14	1145.59	✓	✓

Table V summarizes the number of transient constraints and required simulations under different approaches. As shown in Table V, DT does not introduce explicit transient constraints because it classifies operating points based on stability information rather than enforcing individual transient limits within the optimization process, yet it requires a relatively large number of time-domain simulations, namely 500 runs, to prepare the dataset for training the classifier. By contrast, 2nd-order TS generates a very large number of explicit transient constraints, reaching 4680, although the number of required simulations remains limited. The PCE-based method, combined with the proposed constraint reduction strategy, achieves a more favorable balance: when the expansion order increases from 1 to 3, the number of explicit transient constraints is progressively reduced from 59 to 42, while the number of required simulations grows only from 3 to 10. These results

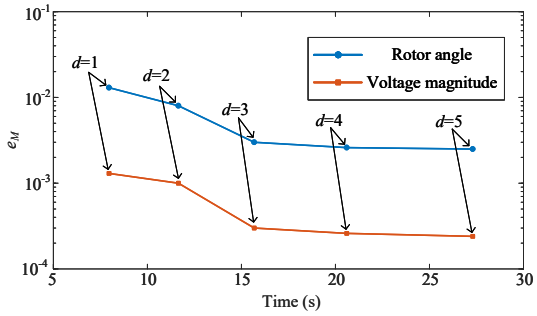

Fig. 7. Error index of moments of the proposed method with different expansion order d in evaluating δ_2 and V_9.

demonstrate that the PCE approach effectively identifies the critical constraints, thereby alleviating the size of the optimization model.

TABLE V
COMPARISON OF NUMBER OF TRANSIENT CONSTRAINTS AND SIMULATIONS

Method	Number of transient constraints	Number of simulations
DT	-	500
2nd-order TS	4680	6
PCE, $d = 1$	59	3
PCE, $d = 2$	45	6
PCE, $d = 3$	42	10

To quantitatively and comprehensively compare the accuracy of different orders of PCE from a statistical perspective, the following error index of moments e_M is defined:

$$e_M = \sqrt{\sum_{j=1}^{2}\left[\sum_{i=1}^{N_t}\left|\frac{M^{(j)}(t_i) - \tilde{M}^{(j)}(t_i)}{M^{(j)}(t_i)}\right|\frac{1}{N_t}\right]^2}, \quad (26)$$

where $M^{(j)}$ and $\tilde{M}^{(j)}$ are the j-th actual and estimated central moments of the system response. The first and second central moments, namely the mean and variance, are considered.

Fig. 7 illustrates the trade-off between computational burden and estimation accuracy of the proposed method under different expansion orders, presented in semilogarithmic scale. It can be observed that increasing the order from 1 to 3 leads to a significant improvement in accuracy, whereas further raising the order offers only marginal gains while the computational burden grows considerably. It is also worth noting that the increase in computational burden becomes more pronounced at higher expansion orders. For example, when the order increases from 1 to 2, the number of required time-domain simulations rises from 3 to 6. By contrast, when the order increases from 4 to 5, the simulations grow from 15 to 21. The 3rd-order PCE achieves sufficient accuracy to simultaneously satisfy the transient constraints on rotor angle and voltage magnitude. Therefore, the 3rd-order expansion provides the most appropriate balance between accuracy and efficiency.

B. IEEE 300-Bus System

We use this case to illustrate the ability of the proposed PCE-based method to approximate and control more state

and algebraic variables that potentially violate the stability constraints in a larger system. The detailed data and the topology of the IEEE 69-machine, 300-bus system can be found in [28] and [33], respectively. The fault is set as a three-phase fault occurring at bus 4 at $t = 0.5$ s, and subsequently cleared by tripping line 4-16 after 0.15 s.

The controllable generators include all generators in the system except for the generator connected to the reference bus. The hyperbolic truncation scheme is employed to alleviate the curse of dimensionality caused by the large amount of control variables. Since this truncation scheme is not the contribution of this paper, further details can be found in [34]. By eliminating the cross terms, the number of required simulations is reduced significantly. Admittedly, the truncation process introduces a certain degree of accuracy degradation. However, as the same truncation scheme is consistently applied to both PCE and the finite difference-based 2nd-order TS because both of them suffer from the curse of dimensionality, it ensures a rigorous and unbiased comparison of their respective approximation accuracies. The initial OP $\boldsymbol{P}_{G0}$ is the original active power injection of the controllable generators and the controllable range is $[90\%\boldsymbol{P}_{G0}, 110\%\boldsymbol{P}_{G0}]$. The steady-state and transient constraint settings are the same as in the previous case except $t_d = 0$ because the employed control measures are capable of restoring the voltage above the transient limits immediately after fault clearance. The reference cost coefficients of generators are utilized as provided in the benchmark [28], maintaining consistency with established practices for the larger system model. The rotor angle of the generator at bus 76 (δ_{76}) and the voltage magnitude of bus 42 (V_{42}) are selected as representatives.

Tables VI and VII show the MAPE comparison of PCE and the 2nd-order TS under different OPs. The farther the OP is from $\boldsymbol{P}_{G0}$, the lower the accuracy of the 2nd-order TS, while the accuracy of PCE is stable, as expected. In addition, for PCE, an increase in d leads to an increase in the accuracy of the approximation of state and algebraic variables, as expected. Meanwhile, the 3rd-order PCE achieves the highest accuracy.

TABLE VI
MAPE OF TRAJECTORIES OF δ_{76} IN THE 2ND-ORDER TS AND DIFFERENT ORDERS OF PCE

Method	$e_{\delta_{76}}$			
	$90\%\boldsymbol{P}_{G0}$	$95\%\boldsymbol{P}_{G0}$	$105\%\boldsymbol{P}_{G0}$	$110\%\boldsymbol{P}_{G0}$
2nd-order TS	4.04%	1.20%	0.94%	2.55%
PCE, d=1	7.21%	2.75%	1.96%	5.37%
PCE, d=2	2.59%	1.14%	0.92%	0.98%
PCE, d=3	0.47%	0.53%	0.31%	0.33%

TABLE VII
MAPE OF TRAJECTORIES OF V_{42} IN THE 2ND-ORDER TS AND DIFFERENT ORDERS OF PCE

Method	$e_{V_{42}}$			
	$90\%\boldsymbol{P}_{G0}$	$95\%\boldsymbol{P}_{G0}$	$105\%\boldsymbol{P}_{G0}$	$110\%\boldsymbol{P}_{G0}$
2nd-order TS	0.67%	0.25%	0.20%	0.91%
PCE, d=1	1.03%	0.52%	0.43%	1.28%
PCE, d=2	0.33%	0.27%	0.15%	0.29%
PCE, d=3	0.09%	0.14%	0.09%	0.16%

Table VIII summarizes the results before and after applying the transient constraint reduction strategy. Because there are more critical machines and buses in this case, more constraints are preserved than in the previous case. It is worth noting that in this case, the total number of transient constraints reaches more than 86000. Although CONOPT in GAMS is capable of handling constraint sets of this magnitude, the computational burden would escalate significantly for larger systems if no reduction strategy is employed. More critically, an excessive number of transient constraints may exceed the solver's computational capacity, potentially leading to infeasibility or numerical instability in the optimization process. Furthermore, the discarded constraints correspond to generator angles or bus voltages whose polynomial surrogate representations remain strictly within admissible limits for all control variable realizations. Consequently, their elimination does not compromise the final optimization outcome.

TABLE VIII
COMPARISON BEFORE AND AFTER APPLYING TRANSIENT CONSTRAINT REDUCTION STRATEGY

Method	Number of transient constraints			
	δ		V	
	Before	After	Before	After
PCE, d=1		5379		11375
PCE, d=2	16215	5238	70500	11146
PCE, d=3		5066		10921

Table IX shows stability and cost results using different methods. From Table IX, it can be observed that while the OOPs obtained from the base OPF, the 2nd-order TS method, and both the 1st- and 2nd-order PCE methods result in lower operational costs, they fail to simultaneously satisfy transient stability requirements. This limitation arises due to the insufficient approximation accuracy of these methods in capturing the nonlinear dynamic behavior of the system. In contrast, only the 3rd-order PCE successfully ensures both rotor angle and voltage transient stability, demonstrating its superior capability in accurately modeling system dynamics.

TABLE IX
STABILITY AND COST RESULTS

Method	Stability		Cost (10^6\$/h)
	δ	V	
Base OPF	✗	✗	1.07277
2nd-order TS	✓	✗	1.09062
PCE, $d = 1$	✗	✗	1.08534
PCE, $d = 2$	✓	✗	1.09099
PCE, $d = 3$	✓	✓	1.10136

Figures 8 and 9 show the trajectories of rotor angles and voltage magnitudes starting from the OOPs of base OPF and 3rd-order PCE, respectively. The trajectories of the rotor angle in Fig. 9 are far from the limit, while those of voltage magnitude are close to the limit indicates that the SR of voltage magnitudes is smaller around the OOP. Figures 8 and 9 show that, while the base OPF solution leads to rotor angle and voltage limit violations, the 3rd-order PCE-based solution avoids these violations. Figures 8 and 9 also show the qualitative difference between these two operating points in terms of transient performance.

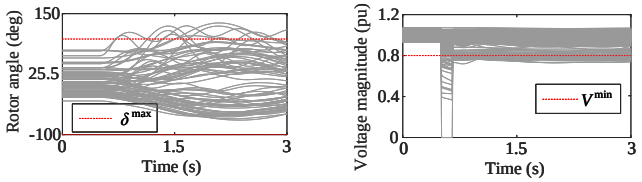

(a) rotor angles (b) voltage magnitudes

Fig. 8. Rotor angles and voltage magnitudes for base OPF.

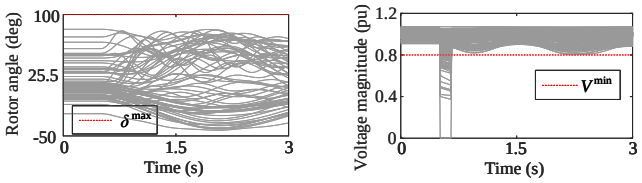

(a) rotor angles (b) voltage magnitudes

Fig. 9. Rotor angles and voltage magnitudes for 3rd-order PCE.

Fig. 10 shows the computation time versus the precision of different orders of the proposed method in semilogarithmic coordinates. As shown in Fig. 10, a significant improvement in estimation accuracy is observed when the expansion order d is increased from the 1st to the 3rd order. However, further increases in the expansion order do not yield substantial improvements in accuracy, while the computational time continues to rise rapidly. At the 3rd order, the transient constraints on both rotor angle and voltage magnitude are satisfied simultaneously. Therefore, based on a balance between estimation accuracy and computational efficiency, the 3rd-order expansion is considered the most suitable choice in the context of this case.

Table X summarizes the computational burdens. It can be seen that the base OPF achieves the highest calculation speed because a large amount of transient stability constraints are ignored. In the time-domain simulation (TDS) stage, the time consumption of the 2nd-order TS and PCE are similar because both methods are essentially quadratic approximations. The number of required time-domain simulations increases approximately linearly with the PCE expansion order when using the hyperbolic truncation scheme. Therefore, the computational burden of the TDS stage increases accordingly. Specifically, 69 simulations are required for 1st-order, 137 for 2nd-order, and 205 for 3rd-order PCE. Compared with the full tensor-product

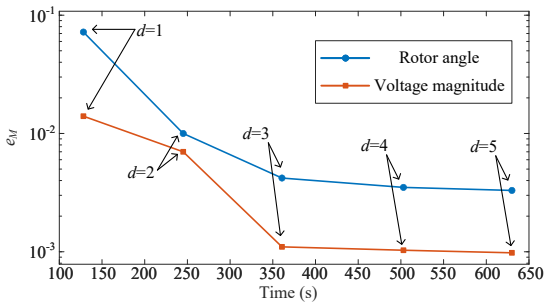

Fig. 10. Error index of moments of the proposed method with different expansion order d in evaluating δ_{76} and V_{42}.

expansion without truncation, which requires 69, 2415, and 57155 simulations for 1st- to 3rd-order PCE, respectively, the truncation scheme eliminates higher-order interaction terms among control variables, substantially reducing the total number of simulations and improving computational tractability. In the optimization stage, by implementing the proposed transient constraint reduction strategy, PCE achieves higher efficiency than the 2nd-order TS. As a result, although the 3rd-order PCE takes the longest time, it provides an effective solution. In addition, although the proposed algorithm is designed for offline implementation, it is important to note that it is intended for "preventive" control. In practical power systems, operators typically perform short-term analyses every 15 to 30 minutes. Thus, despite the computational demands of the proposed method, the computational burden is considered acceptable in real-world applications. Additionally, during the time-domain simulation stage, which accounts for the majority of the computational burden, the simulations are independent of one another inherently. This independence allows for the straightforward implementation of parallel computing frameworks, which could further enhance computational efficiency.

TABLE X
COMPUTATIONAL BURDEN RESULTS

Method	Computational burden (s)		
	TDS stage	Optimization stage	Total
Base OPF	—	0.63	0.63
2nd-order TS	237.07	47.38	284.45
PCE, $d = 1$	121.60	6.62	128.22
PCE, $d = 2$	236.43	8.65	245.08
PCE, $d = 3$	349.26	11.49	360.75

V. CONCLUSIONS

This paper proposes a PCE-based TSC-OPF approach to accurately assess the dynamic response and provide reliable preventive control so that the operating point achieves economic and transient rotor angle and short-term voltage stability simultaneously. The DAEs constraints of the dynamic system are eliminated by substituting the objective function, steady-state, and transient constraints with a set of polynomials of control variables. This process is nonintrusive which provides ease of use for utility companies. In addition, a transient constraint reduction strategy is embedded to significantly reduce the number of constraints which improves the efficiency.

Numerical results clearly demonstrate the effectiveness of the proposed method in solving the TSC-OPF problem. Regarding the 9-bus system, the DT and the proposed 3rd-order PCE are the only approaches that simultaneously satisfy both transient rotor angle and voltage constraints. The corresponding operating costs are 1146.06 \$/h for the DT and 1145.59 \$/h for the 3rd-order PCE, with the latter demonstrating superior economic performance. Although the 2nd-order TS approach achieves a lower cost of 1144.87 \$/h, it fails to satisfy the transient voltage constraints. Moreover, by applying the proposed reduction strategy, the number of transient constraints in the 3rd-order PCE is decreased from 4680 to 42, which substantially reduces the dimensionality of the reformulated optimization problem. In the 300-bus system,

although the 3rd-order PCE yields a higher operating cost of 1.10136×10^6 \$/h compared with 1.09062×10^6 \$/h under the 2nd-order TS approach, only the 3rd-order PCE is able to simultaneously satisfy both transient rotor angle and voltage constraints, whereas the 2nd-order TS method ensures rotor angle stability only. In addition, the 3rd-order PCE requires 205 time-domain simulations, which is larger than the number required by the 2nd-order TS and leads to a longer simulation stage. Nevertheless, the adoption of the proposed constraint reduction strategy substantially decreases the computational burden in the optimization stage, where the solution time is reduced to 11.49 s, significantly shorter than the 47.38 s required by the 2nd-order TS approach.

Future work includes investigating preprocessing techniques to facilitate the integration of PCE into transient stability analysis, with particular emphasis on improving the accuracy of stability boundary characterization. Also, future work involves testing the proposed methodology on electromagnetic transient models that include more nonlinear elements. Other directions for future work include extending the framework to account for model variations induced by non-uniform operational constraints, such as ramping limits and the activation of reactive power controller limits as well as for scenarios with dynamic generator control actions in the post-fault stage.

REFERENCES

[1] Y. Xu, Y. Chi, and H. Yuan, *Stability-constrained optimization for modern power system operation and planning*. John Wiley & Sons, 2023.

[2] J. U. Sevilla-Romero, A. Pizano-Martínez, C. R. Fuerte-Esquivel, and R. Ramírez-Betancour, "Two-stage transient-stability-constrained optimal power flow for preventive control of rotor angle stability and voltage sags," *Journal of Modern Power Systems and Clean Energy*, vol. 12, no. 5, pp. 1357–1369, 2023.

[3] R. Zárate-Miñano *et al.*, "Securing transient stability using time-domain simulations within an optimal power flow," *IEEE Trans. on Power Systems*, vol. 25, no. 1, pp. 243–253, 2009.

[4] J. W. Cruz, J. C. López, D. Dotta, and M. J. Rider, "N-1 multi-contingency transient stability constrained ac optimal power flow with volt/var controllers," *EPSR*, vol. 188, p. 106526, 2020.

[5] F. W. Liederer, J. C. López, M. J. Rider, and D. Dotta, "Transient stability constrained optimal power flow considering fourth-order synchronous generator model and controls," *EPSR*, vol. 213, p. 108667, 2022.

[6] Y. Sun, Y. Xinlin, and H. Wang, "Approach for optimal power flow with transient stability constraints," *IEE Proceedings-Generation, Transmission and Distribution*, vol. 151, no. 1, pp. 8–18, 2004.

[7] G. Geng, V. Ajjarapu, and Q. Jiang, "A hybrid dynamic optimization approach for stability constrained optimal power flow," *IEEE Transactions on Power Systems*, vol. 29, no. 5, pp. 2138–2149, 2014.

[8] S. Xia, Z. Ding, M. Shahidehpour, K. W. Chan, S. Bu, and G. Li, "Transient stability-constrained optimal power flow calculation with extremely unstable conditions using energy sensitivity method," *IEEE Transactions on Power Systems*, vol. 36, no. 1, pp. 355–365, 2020.

[9] A. Pizano-Martínez, C. R. Fuerte-Esquivel, E. A. Zamora-Cárdenas, and J. M. Lozano-García, "Directional derivative-based transient stability-constrained optimal power flow," *IEEE Transactions on Power Systems*, vol. 32, no. 5, pp. 3415–3426, 2016.

[10] T. B. Nguyen and M. Pai, "Dynamic security-constrained rescheduling of power systems using trajectory sensitivities," *IEEE Trans. on Power Systems*, vol. 18, no. 2, pp. 848–854, 2003.

[11] S. Geng and I. A. Hiskens, "Second-order trajectory sensitivity analysis of hybrid systems," *IEEE Trans. on Circuits and Systems I: Regular Papers*, vol. 66, no. 5, pp. 1922–1934, 2019.

[12] H. Choi, P. J. Seiler, and S. V. Dhople, "Propagating uncertainty in power-system dae models with semidefinite programming," *IEEE Trans. on Power Systems*, vol. 32, no. 4, pp. 3146–3156, 2016.

[13] J.-K. Kim and K. Hur, "On the perturbation size of the finite difference method for trajectory sensitivity-based assessment of power system dynamics with non-smooth behavior," *Int. J. of Electrical Power & Energy Systems*, vol. 155, p. 109647, 2024.

[14] R. Mukherjee and A. De, "Development of an ensemble decision tree-based power system dynamic security state predictor," *IEEE Systems Journal*, vol. 14, no. 3, pp. 3836–3843, 2020.

[15] G. N. Baltas, P. Mazidi, F. Fernandez, and P. Rodríguez, "Support vector machine and neural network applications in transient stability," in *Int. Conf. on Renewable Energy Research and Applications (ICRERA)*. IEEE, 2018, pp. 1010–1015.

[16] T. Liu *et al.*, "A bayesian learning based scheme for online dynamic security assessment and preventive control," *IEEE Trans. on Power Systems*, vol. 35, no. 5, pp. 4088–4099, 2020.

[17] T. Su, J. Zhao, and X. Chen, "Deep sigma point processes-assisted chance-constrained power system transient stability preventive control," *IEEE Trans. on Power Systems*, vol. 39, no. 1, pp. 1965–1978, 2023.

[18] H. Jia, Q. Hou, P. Yong, Y. Liu, N. Zhang, D. Liu, and M. Hou, "Voltage stability constrained operation optimization: An ensemble sparse oblique regression tree method," *IEEE Trans. on Power Systems*, vol. 39, no. 1, pp. 160–171, 2023.

[19] N. Zhang *et al.*, "Data-driven security and stability rule in high renewable penetrated power system operation," *Proceedings of the IEEE*, vol. 111, no. 7, pp. 788–805, 2022.

[20] Y. Xu *et al.*, "Propagating uncertainty in power system dynamic simulations using polynomial chaos," *IEEE Trans. on Power Systems*, vol. 34, no. 1, pp. 338–348, 2018.

[21] B. Xia, H. Wu, W. Yang, L. Cao, and Y. Song, "Parametric transient stability constrained optimal power flow solved by polynomial approximation based on the stochastic collocation method," *Energies*, vol. 15, no. 11, p. 4127, 2022.

[22] C. Cui and Z. Zhang, "Stochastic collocation with non-gaussian correlated process variations: Theory, algorithms, and applications," *IEEE Trans. on Components, Packaging and Manufacturing Technology*, vol. 9, no. 7, pp. 1362–1375, 2018.

[23] D. Xiu, *Numerical methods for stochastic computations: a spectral method approach*. Princeton university press, 2010.

[24] X. Li, C. Liu, C. Wang, and F. Milano, "Arbitrary polynomial chaos-based power system dynamic analysis with correlated uncertainties," *Int. J. of Electrical Power & Energy Systems*, vol. 157, p. 109806, 2024.

[25] M. Fan *et al.*, "Uncertainty evaluation algorithm in power system dynamic analysis with correlated renewable energy sources," *IEEE Trans. on Power Systems*, vol. 36, no. 6, pp. 5602–5611, 2021.

[26] P. S. Kundur and O. P. Malik, *Power system stability and control*. McGraw-Hill Education, 2022.

[27] P. W. Sauer, M. A. Pai, and J. H. Chow, *Power system dynamics and stability: with synchrophasor measurement and power system toolbox*. John Wiley & Sons, 2017.

[28] I. Abdulrahman, "Matlab-based programs for power system dynamic analysis," *IEEE Open Access Journal of Power and Energy*, vol. 7, pp. 59–69, 2019.

[29] R. D. Zimmerman *et al.*, "Matpower: Steady-state operations, planning, and analysis tools for power systems research and education," *IEEE Trans. on power systems*, vol. 26, no. 1, pp. 12–19, 2010.

[30] D. Gan, R. J. Thomas, and R. D. Zimmerman, "Stability-constrained optimal power flow," *IEEE Trans. on Power Systems*, vol. 15, no. 2, pp. 535–540, 2000.

[31] X. Li, Z. Li, L. Guan, L. Zhu, and F. Liu, "Review on transient voltage stability of power system," in *2020 IEEE Sustainable Power and Energy Conference (iSPEC)*. IEEE, 2020, pp. 940–947.

[32] C. Liu, K. Sun, Z. H. Rather, Z. Chen, C. L. Bak, P. Thøgersen, and P. Lund, "A systematic approach for dynamic security assessment and the corresponding preventive control scheme based on decision trees," *IEEE Transactions on Power Systems*, vol. 29, no. 2, pp. 717–730, 2013.

[33] A. R. Al-Roomi, "Power Flow Test Systems Repository," Halifax, Nova Scotia, Canada, 2015. [Online]. Available: https://al-roomi.org/power-flow

[34] S. Marelli and B. Sudret, "Uqlab: A framework for uncertainty quantification in matlab," in *Vulnerability, uncertainty, and risk: quantification, mitigation, and management*, 2014, pp. 2554–2563.